



NJC

**Cesium salts of niobo-tungstate isopolyanions with
intermediate group V - group VI character**

Journal:	<i>New Journal of Chemistry</i>
Manuscript ID	NJ-ART-10-2015-002914.R1
Article Type:	Paper
Date Submitted by the Author:	17-Nov-2015
Complete List of Authors:	Sures, Dylan; Oregon State University, Chemistry Molina, Pedro; Oregon State University, Chemistry Miro, Pere; University of Minnesota, Department of Chemistry Zakharov, Lev; Oregon State University, Department of Chemistry Nyman, May; Oregon State University,

SCHOLARONE™
Manuscripts



Cite this: DOI: 10.1039/xxxxxxxxxx

Cesium salts of niobo-tungstate isopolyanions with intermediate group V - group VI character[†]

Dylan J. Sures,^a Pedro I. Molina,^a Pere Miró,^b Lev N. Zakharov,^a and May Nyman^{*a}

Received Date

Accepted Date

DOI: 10.1039/xxxxxxxxxx

www.rsc.org/journalname

Alkali metal salts of polyoxometalates (POMs) of the group VI elements (W and Mo) and polycoltanates (Nb and Ta POMs) exhibit opposing trends in their solubility in water and ion-association in solution. Mixed clusters of these two group V metals and tungsten provide an opportunity to probe the reversal in these trends and to understand their origin. A review of a classic study of mixed Nb/W clusters and our own work in Ta/W polyanions, have led us to isolate Cs⁺/Na⁺ salt of [Nb₄W₂O₁₉]⁶⁻ and two salts, Cs⁺/Na⁺ and pure Cs⁺, of [Nb₂W₄O₁₉]⁴⁻ by using peroxoniobate ([Nb(O₂)₄]³⁻) instead of hexaniobate ([Nb₆O₁₉]⁸⁻) as the niobium source. Crystallographic analysis shows that Cs⁺-bonding to clusters increases with Nb-content, following the trend observed in our previous studies of hexaniobate in solution. Fragmentation by ESI-MS suggests that niobium-rich [Nb₄W₂O₁₉]⁶⁻ is less stable than isostructural [Nb₂W₄O₁₉]⁴⁻ and this technique, together with FTIR, confirms the predominance of the cis- isomer in the cluster structures. The mixed-metal composition of these isopolyanions is reflected in the crystallographic bond lengths and in the positions of the absorption bands in the UV spectra. DFT calculations reveal that the HOMO-LUMO energy gap widens with increasing Nb content in the cluster framework – an effect ascribed to the overall poorer mixing of Nb_{4d}, versus W_{5d}, atomic orbitals with the corresponding O_{2p} orbitals.

1 Introduction

Ion-association is an extremely important phenomenon in natural and synthetic aqueous systems. The relationship between ions defines the structural transition between the solid and aque-

ous states of ionic materials and directly influences their self-assembly, as well as the solubility and stability of related compounds in solution. Alkali salts of polyoxometalates (POMs) provide a unique opportunity to study these processes. POMs are discrete anionic metal-oxo clusters of the early *d*⁰ transition metals (W^{VI}, Mo^{V/VI}, V^V, Nb^V, Ta^V).¹ This family of clusters displays a range of functional properties² and may be divided into two distinct subsets with regard to their predominant self-assembly conditions, redox chemistry, charge density, and solubility properties. Group VI POMs (W^{VI} and Mo^{V/VI}) self-assemble via acidification of aqueous solutions, possess low charge-density, and exhibit rich redox chemistry. Group V (Nb^V and Ta^V) POMs are predominantly assembled and stable in base and possess poor redox character, consistent with their highly negative charge-densities.³ Meanwhile, V^V POMs have properties closer to those of Group VI POMs, exemplified by their rich redox character and acidic self-assembly conditions.

A crucial and less commonly recognized difference between these two classes of POMs can be seen in their solubilities with

^a Department of Chemistry, Oregon State University, 107 Gilbert Hall, Corvallis, OR, 97331-4003, USA

^b Department of Physics and Earth Sciences, Theoretical Physics – Theoretical Material Science, Jacobs University, Bremen, Germany

* To whom general correspondence should be addressed:

may.nyman@oregonstate.edu

Website: <http://nyman.chem.oregonstate.edu/>

[†] Electronic Supplementary Information (ESI) available: Crystallographic data, TGA, FTIR, Group Theory Analysis, SEM/EDX, ESI-MS, BVS, and additional computational details and tables. The crystallographic information files (cif) are deposited in the Cambridge Crystallographic Data Centre (CCDC, Cambridge, United Kingdom) – CCDC 1347129 (CsNa{Nb₂W₄}), CCDC 1347130 (Cs{Nb₂W₄}), and CCDC 1437131 (CsNa{Nb₄W₂}) and the Inorganic Crystal Structure Database (ICSD, Karlsruhe, Germany) – CSD-430334 (CsNa{Nb₂W₄}), CSD-430336 (Cs{Nb₂W₄}), and CSD-430335 (CsNa{Nb₄W₂}). For ESI and crystallographic data in CIF or other electronic format, see See DOI: 10.1039/b000000x/

respect to charge-balancing counteranions. Group VI POMs exhibit solubility related to the hydration sphere and solvation energy of their cations, with Li-salts being the most soluble and Cs-salts being the least soluble. Likewise, this is the accepted 'normal' solubility trend for simple salts in water, since hydration of ions is the thermodynamic driving force for aqueous dissolution.⁴ Conversely, Group V POMs of Nb and Ta have the opposite solubility trend, with greater cationic radius resulting in enhanced solubility, while polyvanadates exhibit solubility trends more typical of Group VI POMs.^{5–8} Given the distinct differences between POM chemistry of Nb & Ta compared to V, we have previously coined the term 'polycoltanate' (derived from coltan, abbreviation of columbite-tantalite – the ore from which Nb and Ta are extracted) to explicitly mean the POM chemistry of Nb & Ta.⁹ This reverse solubility phenomenon of polycoltanates with counterions was initially recognized with the hexaniobate Lindqvist ion, $[\text{Nb}_6\text{O}_{19}]^{8-}$ – the most persistent aqueous species of sufficiently alkaline solutions of niobium oxide.^{10,11} Understanding and exploiting this unusual trend remains a worthwhile goal, allowing us to more efficiently perform separations, assembly, and manipulation of inorganic materials in water. Moreover, there is particular interest in developing technologies for separating and sequestering Cs^+ , since ^{137}Cs remains the biggest challenge of legacy nuclear wastes, as well as the radionuclide of greatest concern in the more recent Fukushima nuclear disaster.¹²

A large number of metals¹³ and even non-metals¹⁴ can replace W^{VI} and Mo^{VI} in Group VI POMs. This strategy has increased the range of the properties of these polyanions.^{15,16} An illustrative example of this approach is displayed by the synthesis of the Nb-substituted series of hexatungstate ($[\text{W}_6\text{O}_{19}]^{2-}$).¹⁷ This compositional series of Lindqvist-type Nb/W isopolyanions, $[\text{Nb}_x\text{W}_{6-x}\text{O}_{19}]^{(2+x)-}$ ($x = 1-4$), was originally prepared 40 years ago by Dabbabi et al. from reactions of $\text{K}_8[\text{Nb}_6\text{O}_{19}]$ and sodium tungstate in aqueous media under pH control and in the presence of H_2O_2 .¹⁸ The original report did not include crystallographic analysis of the structures and just $[\text{NbW}_5\text{O}_{19}]^{3-}$ (as the TMA^+/K^+ ¹⁹, and the TBA^+ salt²⁰), $[\text{Nb}_2\text{W}_4\text{O}_{19}]^{4-}$ ²¹, and a hybrid derivative of the latter²² have been structurally characterized so far. These highly symmetric clusters with mixed metal site occupancies present significant disorder, rendering proper structure interpretation challenging, but Cs^+ may provide the advantage of orienting the clusters by preferred coordination to the more basic niobium-bonded oxo-ligands. More importantly, prior studies comparing arrangement of ions in the solid-state to their ion-association in solution have presented an emerging trend that solution behavior remarkably mirrors solid-state structure.^{6,23–25} Structural characterization of these mixed metal POMs is thus a worthwhile effort as a foundation for future solution studies that focus specifically on ion-association and solubility.

This series of niobo-tungstate POMs bridging end-member

Group V and Group VI clusters allows for insight into an intermediate set of trends in self-assembly and ion-pairing. Increasingly alkaline reaction conditions result in gradual Nb substitution for W centers, exemplifying the hybrid nature of these POMs.¹⁸ The Cs^+ salts of the members of this series are of particular interest from an ion-association perspective, due to the stark contrast between the extreme solubility of $\text{Cs}_8[\text{Nb}_6\text{O}_{19}]$ (as high as 1.5 molar) and the insolubility of Cs^+ polytungstates. Here we complement structural data with electrospray ionization mass spectroscopy (ESI-MS), vibrational spectroscopies, and compositional analysis to determine compositional and isomeric purity of the Lindqvist ions. UV-vis spectroscopy corroborated with simulations elucidate the origin of shifting HOMO-LUMO gaps with composition.

2 Experimental

2.1 Syntheses

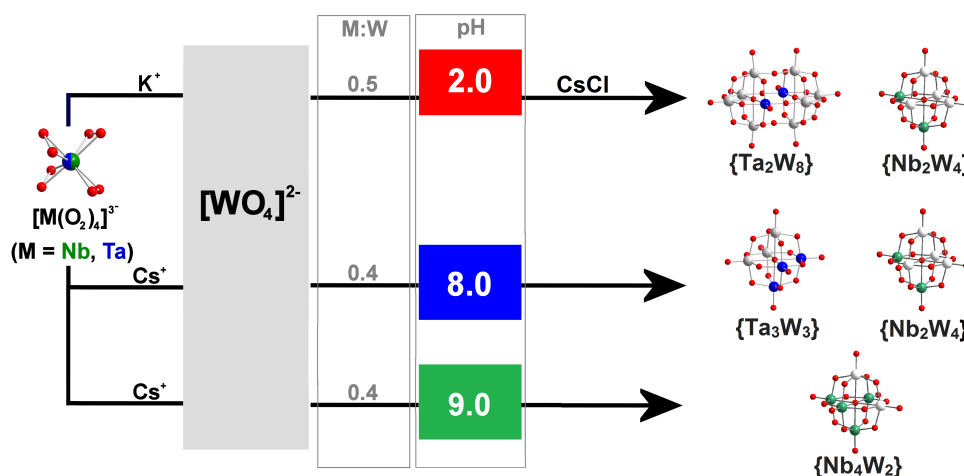
Synthesis of the three reported compounds is detailed below, and instrumentation and additional crystallographic details are available in the Supplementary Information.

2.1.1 $\text{Cs}_4\text{Na}_2[\text{Nb}_4\text{W}_2\text{O}_{19}] \cdot 12\text{H}_2\text{O}$ ($\text{CsNa}\{\text{Nb}_4\text{W}_2\}$)

$\text{Na}_2\text{WO}_4 \cdot 2\text{H}_2\text{O}$ (3.3 grams, 10.0 mmol) was added to 40 mL of H_2O at room temperature and stirred until dissolution. $\text{Cs}_3[\text{Nb}(\text{O}_2)_4]$ (2.9 grams, 4.7 mmol) was added to the solution, which was further stirred for 10 minutes. The suspension was then slowly acidified dropwise with 12 M HCl until the pH reached a value of 9, during which a white precipitate formed and redissolved. The solution was then refluxed for 4 h, microfiltered with a 0.45 μm nylon syringe filter, cooled to room temperature, and allowed to crystallize at 4 °C. Macroscopic colorless block-like crystals formed after 60 hours. The mother liquor was removed and the crystals were washed in 2-propanol and dried under vacuum.

Yield = 0.604 grams (27.6% by mass). Full formula: $\text{Cs}_4\text{Na}_2\text{Nb}_4\text{W}_2\text{O}_{31}\text{H}_{24}$. MW = 1838.8 g mol^{-1} . Atomic Ratios, calculated (found): W/Nb: 0.5 (0.5), Cs/Nb: 1.0 (1.0), Cs/W: 2.0 (2.1). Characteristic IR bands (cm^{-1}): 531 (s,br), 733 (s, br), 840 (s, sh), 874 (w), 884 (m), 907 (m, sh), 932 (m, sh). UV absorption: $\lambda_1 = 211 \text{ nm}$, $\epsilon_1 = 1.87 \times 10^5 \text{ L mol}^{-1} \text{ cm}^{-1}$, λ_2 ($n(\text{O}_b) \rightarrow \pi^*(\text{M}-\text{O}_b)$ transfer band) = 253 nm, $\epsilon_2 = 1.51 \times 10^5 \text{ L mol}^{-1} \text{ cm}^{-1}$. Water content (%), crystallographic (TGA 22-400 °C, in air): 12.1 (11.84).

Crystallographic Data: $\text{Cs}_4\text{H}_{24}\text{O}_{31}\text{Na}_2\text{Nb}_{3.89}\text{W}_{2.11}$; MW = 1846.70 g mol^{-1} ; Size: (0.16 x 0.14 x 0.08) mm^3 , T = 150 K; crystal system: monoclinic; space group: $\text{P}2_1/n$, $a = 9.5760(3) \text{ \AA}$, $b = 13.5844(4) \text{ \AA}$, $c = 12.3503(4) \text{ \AA}$, $\beta = 90.0790(12)^\circ$, V = 1606.58(9) \AA^3 ; Z = 2; $D_c = 3.817 \text{ mg m}^{-3}$; $\mu = 13.446 \text{ mm}^{-1}$; F(000) = 1659; $2\theta_{\text{max}} = 80.0^\circ$; 45150 reflections; 9955 independent reflections [$R_{\text{int}} = 0.0299$]; $R_1 = 0.0310$, $wR_2 = 0.0917$



Scheme 1 Reaction products for niobo- and tantalotungstates⁹ in analogous conditions. Color code: Nb, green; Ta, blue; W, grey; O, red.

and GOF = 1.260 for 9955 reflections (248 parameters) with $I > 2\sigma(I)$; $R_1 = 0.0318$, $wR_2 = 0.0921$ and GOF = 1.261 for all reflections; max/min residual electron density, $+2.644/-1.995 \text{ e}\text{\AA}^{-3}$.

2.1.2 $\text{Cs}_3\text{Na}[\text{Nb}_2\text{W}_4\text{O}_{19}] \cdot 10\text{H}_2\text{O}$ ($\text{CsNa}\{\text{Nb}_2\text{W}_4\}$)

$\text{Na}_2\text{WO}_4 \cdot 2\text{H}_2\text{O}$ (3.3 grams, 10.0 mmol) was added to 40 mL of H_2O at room temperature and stirred to dissolve. $\text{Cs}_3[\text{Nb}(\text{O}_2)_4]$ (2.9 grams, 4.7 mmol) was added to the solution, which was further stirred for 10 minutes. The suspension was then slowly acidified dropwise with 12 M HCl until the pH reached a value of 8, during which a white precipitate formed and redissolved. The slightly yellow solution was then refluxed for 4 h, microfiltered with a $0.45 \mu\text{m}$ nylon syringe filter, cooled to room temperature, and allowed to crystallize at 4°C . Small silvery-white flake-like crystals formed over two days. The solid was separated by vacuum filtration, washed in 2-propanol, and dried under vacuum.

Yield = 0.210 grams (4.9% by mass) from initial crystallization. More product can be obtained by boiling the mother liquor to half of its initial volume and cooling the solution again to 4°C . Full formula: $\text{Cs}_3\text{NaNb}_2\text{W}_4\text{O}_{29}\text{H}_{20}$. MW = 1827.0 g/mol. Atomic Ratios, calculated (found): W/Nb: 2.00 (1.98), Cs/Nb: 1.50 (1.52), W/Cs: 1.33 (1.30). Characteristic IR bands (cm^{-1}): 488 (vw), 529 (vw), 567 (m), 773 (s, br), 894 (s), 947 (s). UV absorption: $\lambda_1 = 198 \text{ nm}$, $\epsilon_1 = 1.74 \times 10^5 \text{ L mol}^{-1} \text{ cm}^{-1}$, λ_2 ($n(\text{O}_b) \rightarrow \pi^*(\text{M}-\text{O}_b)$ transfer band) = 269 nm, $\epsilon_2 = 1.05 \times 10^5 \text{ L mol}^{-1} \text{ cm}^{-1}$. Water content (%), crystallographic (TGA 22-500 $^\circ\text{C}$, in air): 9.2 (9.15).

Crystallographic Data: $\text{Cs}_3\text{H}_{20}\text{NaO}_{29}\text{Nb}_{2.14}\text{W}_{3.86}$; MW = 1814.67 g/mol, size: (0.09 x 0.07 x 0.04) mm^3 ; T = 173 K; crystal system: trigonal; space group: R3; $a = 11.6472(15) \text{ \AA}$, $b = 11.6472(15) \text{ \AA}$, $c = 19.117(2) \text{ \AA}$, V = 2245.9(6) \AA^3 ; Z = 3; $D_c = 4.025 \text{ mg m}^{-3}$; $\mu = 19.280 \text{ mm}^{-1}$; F(000) = 2404; $2\theta_{\text{max}}$

= 60.0° ; 12477 reflections; 2686 independent reflections [$R_{\text{int}} = 0.0566$]; $R_1 = 0.0325$; $wR_2 = 0.0520$ and GOF = 1.008 for 2686 reflections (122 parameters) with $I > 2\sigma(I)$, $R_1 = 0.0496$, $wR_2 = 0.0563$ and GOF = 1.009 for all reflections; max/min residual electron density: $+1.211/-1.167 \text{ e}\text{\AA}^{-3}$.

2.1.3 $\text{Cs}_4[\text{Nb}_2\text{W}_4\text{O}_{19}] \cdot 4\text{H}_2\text{O}$ ($\text{Cs}\{\text{Nb}_2\text{W}_4\}$)

$\text{Na}_2\text{WO}_4 \cdot 2\text{H}_2\text{O}$ (3.3 grams, 10.0 mmol) was added to 40 mL of H_2O at room temperature and stirred until dissolution. $\text{K}_3[\text{Nb}(\text{O}_2)_4]$ (1.6 grams, 4.7 mmol) was added to the solution, which was further stirred for 10 minutes. The suspension was then slowly acidified dropwise with 12 M HCl, during which a white precipitate formed and redissolved until the pH reached a value of 7. Upon continued dropwise addition of HCl, the solution grew increasingly opaque and yellow until the pH reached a value of 2. The yellow suspension was then refluxed for 2 hours. The resulting solution was allowed to cool to room temperature and was then centrifuged. The supernatant was separated and microfiltered with a $0.45 \mu\text{m}$ nylon syringe filter. 6.0 grams of CsCl were then added to the supernatant and a cream-colored precipitate formed. This precipitate was isolated by centrifugation and removal of the supernatant liquid. The solid was dissolved in the minimum amount of boiling water ($\approx 120 \text{ mL}\cdot\text{g}^{-1}$) and allowed to recrystallize at 4°C . After a day, small needle-like colorless crystals formed. The crystals were washed in 2-propanol and dried under vacuum.

Yield = 1.703 grams (39.6% by mass, crude product). Full formula: $\text{Cs}_4\text{Nb}_2\text{W}_4\text{O}_{23}\text{H}_8$. MW = 1828.84 g/mol. Atomic Ratios, calculated (found): W/Nb: 2.00 (2.02), Cs/Nb: 2.00 (1.93), W/Cs: 1.00 (1.04). Characteristic IR bands (cm^{-1}): 594 (m), 773 (s), 860 (w, sh), 947 (s, sh). UV absorption: $\lambda_1 = 196 \text{ nm}$, $\epsilon_1 = 1.64 \times 10^5 \text{ L mol}^{-1} \text{ cm}^{-1}$, λ_2 ($n(\text{O}_b) \rightarrow \pi^*(\text{M}-\text{O}_b)$ transfer band)

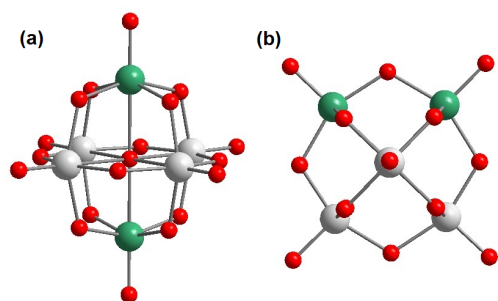


Fig. 1 (a) D_{4h} *trans*-isomer of $\{\text{Nb}_2\text{W}_4\}$. (b) C_{2v} *cis*-isomer of $\{\text{Nb}_2\text{W}_4\}$, viewed along a terminal-oxo bond. Color code: Nb, green; W, grey; O, red.

$\lambda = 271$ nm, $\epsilon_2 = 1.03 \times 10^5$ L mol $^{-1}$ cm $^{-1}$. Water content (%), crystallographic (TGA 22-400 °C, in air): 4.0 (3.95).

Crystallographic Data: Cs $_4$ H $_8$ O $_{31}$ Nb $_{1.97}$ W $_{4.03}$; MW = 1832.11 g mol $^{-1}$, size: (0.16 x 0.14 x 0.08) mm 3 , T = 150 K; crystal system: monoclinic; space group: P2 $_1$ /n, $a = 9.6119(8)$ Å, $b = 11.8087(10)$ Å, $c = 11.2532(9)$ Å, $\beta = 90.929(18)^\circ$, $V = 1277.12(18)$ Å 3 ; Z = 2; $D_c = 4.764$ mg m $^{-3}$; $\mu = 24.655$ mm $^{-1}$; F(000) = 1582; $2\theta_{max} = 86.80^\circ$; 42881 reflections; 9627 independent reflections [$R_{int} = 0.0744$]; $R_1 = 0.0468$, $wR_2 = 0.0869$ and GOF = 1.016 for 9627 reflections (155 parameters) with $I > 2\sigma(I)$, $R_1 = 0.0897$, $wR_2 = 0.1037$ and GOF = 1.016 for all reflections; max/min residual electron density, +5.933/-4.251 eÅ $^{-3}$.

3 Results and Discussion

3.1 Synthetic Variations

Departing from Dabbabi's hexaniobate-based syntheses, peroxoniobate ($[\text{Nb}(\text{O}_2)_4]^{3-}$)²⁶ was used as the Group V metal source for three Cs $^+$ salts of POMs: Cs $_4$ Na $_2$ [Nb $_4$ W $_2$ O $_{19}$] \cdot 12H $_2$ O (CsNa{Nb $_4$ W $_2$ }), Cs $_3$ Na[Nb $_2$ W $_4$ O $_{19}$] \cdot 10H $_2$ O (CsNa{Nb $_2$ W $_4$ }), and Cs $_4$ [Nb $_2$ W $_4$ O $_{19}$] \cdot 4H $_2$ O (Cs{Nb $_2$ W $_4$ }). Peroxide is important for maintaining solubility of niobium in slightly alkaline to acid conditions (*i.e.*, pH < 10). The use of peroxoniobate allows for greater control over these syntheses by providing minimal and consistent peroxide concentration. Peroxide is an unstable molecule with respect to heat, base and redox reactions, leading to potential inconsistent or uncontrolled results. This is particularly true because tungsten is likewise redox active.

The pH of the reaction controlled variance in the Nb:W ratio in each compound, thereby bridging the opposing self-assembly environments of Group V and Group VI POMs and paralleling Dabbabi's pioneering work on the $[\text{Nb}_x\text{W}_{6-x}\text{O}_{19}]^{(2+x)-}$ series.¹⁸ While the general trend of increasing niobium content with higher pH was maintained, the actual pH ranges where members of the series were prevalent shifted with respect to reaction basicity. For instance, with peroxoniobate as the Group V metal source,

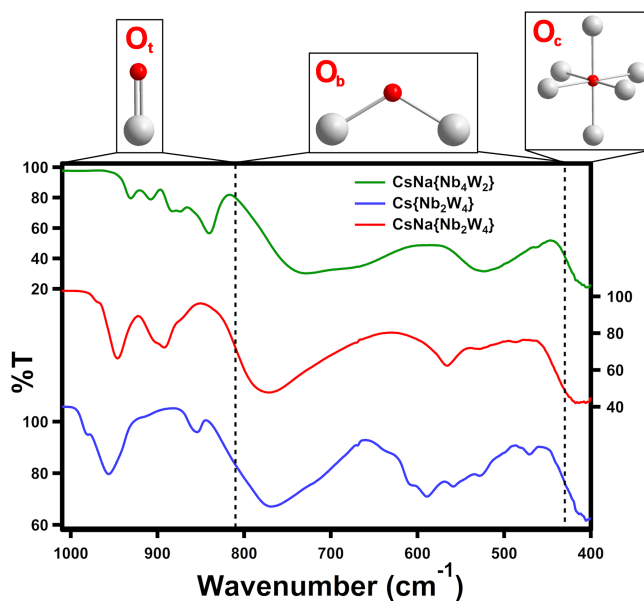


Fig. 2 IR spectra of CsNa{Nb $_4$ W $_2$ }, Cs{Nb $_2$ W $_4$ }, and CsNa{Nb $_2$ W $_4$ }, supporting the existence of more than two IR-active terminal-oxo stretching modes for each compound in the terminal-oxo stretching range. Regions for terminal-oxo stretches, bridging-oxo stretches, and bending modes involving the central-oxo are labeled. The full FTIR spectra are shown in Figure S5.

the $[\text{Nb}_2\text{W}_4\text{O}_{19}]^{4-}$ species is formed at wide pH range ($2 < \text{pH} < 8$) instead of specifically at pH ≈ 5.5 .¹⁸ However, we do need to take into account the crystallizing counteractions, as they can exhibit selectivity for crystallizing specific cluster compositions and isomers.

Scheme 1 summarizes the reaction conditions under which the three reported Lindqvist salts were obtained, along with tantaloniobate clusters from a prior study.⁹ While the Cs{NbW $_9$ } analogue of Cs{TaW $_9$ } was successfully synthesized, attempts at making niobate forms of Cs{Ta $_2$ W $_8$ } and CsNa{Ta $_3$ W $_3$ } instead resulted in Cs{Nb $_2$ W $_4$ } and CsNa{Nb $_2$ W $_4$ }, respectively. CsNa{Nb $_4$ W $_2$ } was obtained by raising the pH from 8 to 9 in the CsNa{Nb $_2$ W $_4$ } reaction.

3.2 Structures

3.2.1 Isomer Determination

We can conclude that the *cis*-isomers of both clusters, {Nb $_4$ W $_2$ } and {Nb $_2$ W $_4$ }, are the main crystalline products from the reaction mixtures. This is suggested by the number of absorption bands in the FTIR spectra (Figure 1).²⁷ Focusing on the prominent terminal-oxo stretches (M-O $_t$) at 850-1000 cm $^{-1}$ (Figure 2), the low-symmetry C_{2v} *cis*-isomer exhibits six IR stretches (A_1 and B_1 from the two-site metal and $2A_1$, B_1 , and B_2 from the four-site metal). On the other hand, the high-symmetry D_{4h} *trans*-isomer

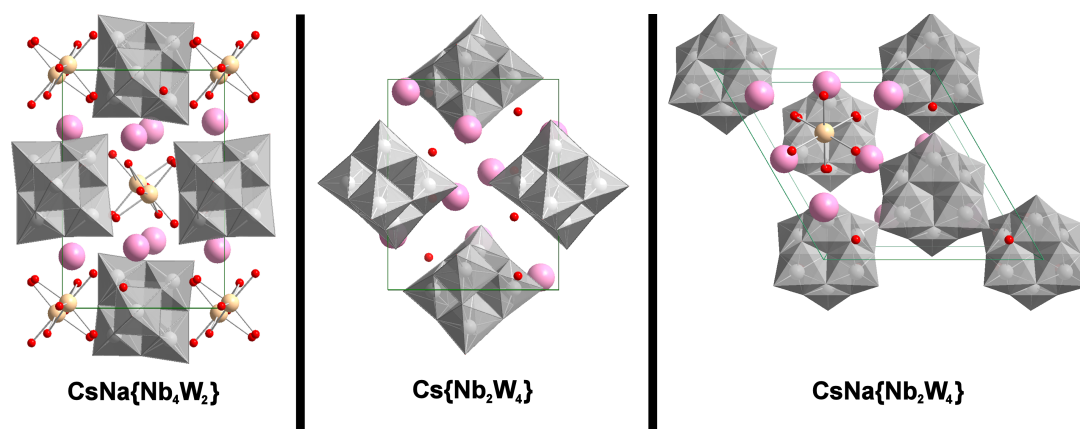


Fig. 3 Representation of the crystal structures of $\text{CsNa}\{\text{Nb}_4\text{W}_2\}$, $\text{Cs}\{\text{Nb}_2\text{W}_4\}$, and $\text{CsNa}\{\text{Nb}_2\text{W}_4\}$ viewed along the crystallographic c axis. Color code: unit cell edges, dark green; MO_6 ($M = \text{Nb}/\text{W}$), grey; Cs^+ , pink and Na^+ , tan; O (from lattice water molecules), red.

Table 1 Nb/W occupancies for each cluster by free refinement of X-ray data and energy dispersive spectroscopy (EDX)

Cluster	Nb/W Occupancy (Free Refinement)	Nb/W Occupancy (EDX)
$\text{CsNa}\{\text{Nb}_4\text{W}_2\}$	3.89/2.11	3.97(3)/2.03(3)
$\text{Cs}\{\text{Nb}_2\text{W}_4\}$	1.97/4/03	1.99(3)/4.01(3)
$\text{CsNa}\{\text{Nb}_2\text{W}_4\}$	2.14/3.86	2.05(4)/3.95(4)

would exhibit only two IR stretches (A_{2u} from the two-site metal and E_u from the four-site metal) (Table S6). All three compounds exhibit more than two IR stretching bands within this region, ruling out the high-symmetry D_{4h} trans structures. Thus, each ion must exist as the lower-symmetry C_{2v} cis-isomer. Although not all six peaks are immediately perceptible in the 850-1000 cm^{-1} region of each IR spectrum, predominance of the D_{4h} structures can be ruled out due to the clear existence of more than two peaks. Computational verification of these assignments is shown in Table S25. Bridging oxygen (M-O_b) stretching modes are primarily responsible for bands in the 500-850 cm^{-1} region. Combinations of bridging oxygen and central oxygen (M-O_c) bending modes result in the bands at lower wavenumbers.²⁷ The disparity between the spectra of the two $\{\text{Nb}_2\text{W}_4\}$ species, most prominently in the 890-910 cm^{-1} range, can be attributed to the additional Cs^+ in $\text{Cs}\{\text{Nb}_2\text{W}_4\}$ associating to additional terminal oxygen atoms on the clusters, weakening their stretching signals (Figure 4).

3.2.2 Crystallographic Structures

In each of the three studied phases, the free refinement of metal occupancies very closely matched the ratios found by energy-dispersive x-ray spectroscopy (EDX, Table 1). The fully-oxidized states of the metals were fixed since there is no evidence (i.e. color) for reduction of W^{VI} and reduction of Nb^{V} is extremely rare in polyanions. Although Bond Valence Sum (BVS) calculations were attempted for all three structures, the degree of mixed-

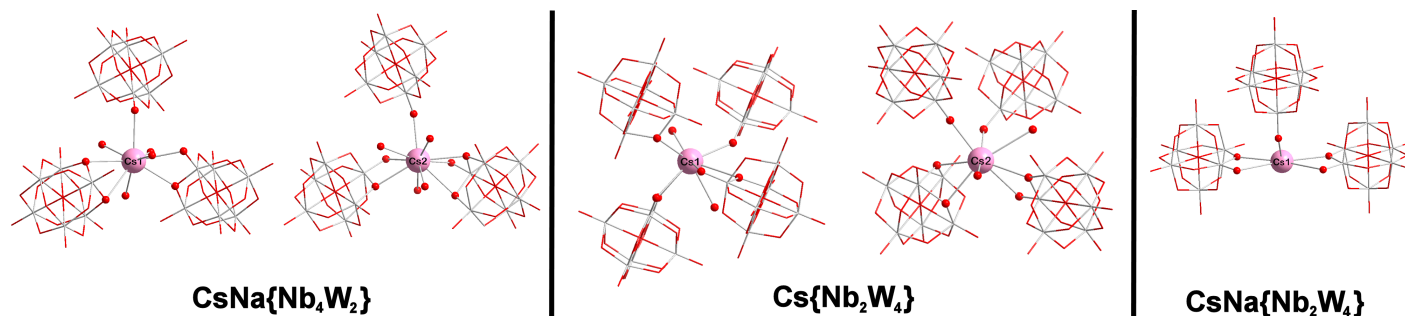
occupancy and disorder in each lattice significantly decreased the effectiveness of such calculations for determining atomic ratios.²⁸⁻³⁰ SEM-EDX was instead employed for this purpose, which is capable of giving very accurate ratios of heavy metals and these analyses confirmed the ratios obtained from free refinement of the site occupancies (Table 1). Additionally, the Nb/W ratios are confirmed by the number of fully-occupied counteranions sites per cluster (six for the case of $\text{CsNa}\{\text{Nb}_4\text{W}_2\}$ and four for the case of both $\{\text{Nb}_2\text{W}_4\}$ structures), due to the requirement for charge-balance. The BVS values of the bridging oxos are strictly greater than 1.720 in all three structures (Tables S16-S18), likewise showing no protonation that would reduce the number of required counteranions. In summary, when coupled with the EDX data, the full occupancy of the counteranions in each structure allows assignment of the metal occupancies to their nearest integer values with confidence.

Both $\text{CsNa}\{\text{Nb}_4\text{W}_2\}$ and $\text{Cs}\{\text{Nb}_2\text{W}_4\}$ crystallize in the orthorhombic crystal system with three symmetrically independent metal sites in the cluster unit (Figure 3). Nb and W are disordered over the six metal positions, with total occupancies summing to match the respective metal ratios in each cluster. The free refinement yielded an Nb/W ratio very close to 2:1 for $\text{CsNa}\{\text{Nb}_4\text{W}_2\}$ and 1:2 for $\text{Cs}\{\text{Nb}_2\text{W}_4\}$ (Table 1). Each of these ratios was supported by the atomic % ratio (EDX) and the crystallographic determination of the number of cations required to fully balance the charge on each cluster (six and four, respectively). $\text{CsNa}\{\text{Nb}_2\text{W}_4\}$ crystallizes in the trigonal space group $R\bar{3}$ with only two symmetrically independent metal sites in the cluster unit. The free refinement again yielded an Nb:W occupancy ratio close to 1:2 and this ratio was further supported by the atomic % ratio, as well as the crystallographically determined number of cations.

In the $\text{CsNa}\{\text{Nb}_4\text{W}_2\}$ structure, Lindqvist ion units are arranged in layers perpendicular to the c -axis. Cs^+ coordinates

Table 2 Summary of metal-oxo bond lengths in Lindqvist ions

Oxo-bond type	{Nb ₆ }	CsNa{Nb ₄ W ₂ }	Cs{Nb ₂ W ₄ }	CsNa{Nb ₂ W ₄ }	{W ₆ }
M-O _t	1.804(9) Å	1.751-1.786 Å	1.726-1.759 Å	1.746-1.752 Å	1.689(6) Å
M-O _b	2.005(2) Å	1.951-1.981 Å	1.915-2.005 Å	1.919-1.991 Å	1.924(3) Å
M-O _c	2.381(1) Å	2.333-2.360 Å	2.341-2.386 Å	2.333-2.337 Å	2.331(4) Å

**Fig. 4** Representation of the coordination environments of the Cs⁺ counteranions in the structures of CsNa{Nb₄W₂}, Cs{Nb₂W₄}, and CsNa{Nb₂W₄}.

to terminal and μ_2 bridging oxygens on the clusters and sodium counteranions bonded to six water molecules each are interspersed between the cluster layers. The values for metal-oxygen distances for each of the three inequivalent oxygen types (Figure S15) fall in the expected range for an Nb/W mixed-metal cluster (Table 2). The bond distances between the mixed-metal sites and the terminal oxo ligands (O_t) are intermediate between those of terminal-oxo bond lengths in hexatungstate ({W₆}) and hexaniobate ({Nb₆}).³¹ The bond lengths are slightly closer to those in {Nb₆}, indicative of the greater Nb than W occupancy in each metal site. This trend is also observed for the bridging oxo bond lengths (M-O_b), which are on average slightly closer to the bond length of Nb-O_b than that of W-O_b. This is again the case for the bonds to the central oxygen (M-O_c). In the Cs{Nb₂W₄} structure, a similar stacking arrangement of Lindqvist ions and counteranions is seen, but with no sodium ions. The metal-oxygen distances for the three oxygen types are within the expected range for an Nb/W mixed cluster, but with bond lengths generally closer to those in {W₆} to reflect the greater tungsten occupancy at each metal site. In CsNa{Nb₂W₄}, the M-O_t and M-O_b bond lengths fall within the ranges in Cs{Nb₂W₄}. The M-O_c bonds have lengths slightly shorter than those in Cs{Nb₂W₄} and closer to those in {W₆}. The inclusion of Nb in the structure of {W₆} therefore typically results in the lengthening of bond distances due to both the lower valency of Nb^V and the mixing of metals in the structure, which typically distorts the molecular framework.

Considering the counteranion coordination environments with respect to only the POMs in the lattice, the two crystallographically distinct Cs⁺ sites in CsNa{Nb₄W₂} exhibit five-coordinate and six-coordinate bonding to the terminal and bridging oxygen

atoms (Figure 4). Each Cs⁺ additionally bridges to the sodium cations in the lattice via four water molecules (for total Cs⁺ coordination numbers of nine and ten). A similar Cs⁺ bonding scheme is seen in Cs{Nb₂W₄} with Cs⁺ exhibiting six-coordinate bonding with respect to the oxygen atoms in their associated clusters (Figure 4). However, solvent water molecules instead bridge Cs⁺, since there is no sodium in the lattice. Cs⁺ sites in CsNa{Nb₂W₄} only have four bonds to the clusters' terminal and bridging oxygen atoms, and the remaining coordination is to water molecules (C.N.=11). Moreover, the bonding of Cs⁺ to the clusters is primarily to the terminal oxos, suggesting the less basic nature of the bridging oxos in these W-rich sites. Meanwhile, Cs-cations of Cs{Nb₂W₄} bond to both bridging and terminal oxos, likely because there is more Cs in the lattice (no sodium) and a surprising lack of lattice water (Figure 4). Alkali-cluster lattices typically contain ten or more water molecules per cluster. In the clusters with sodium counteranions (CsNa{Nb₄W₂} and CsNa{Nb₂W₄}), sodium ions only coordinate to lattice water molecules and exhibit no coordination to cluster oxygen atoms. The cesium-oxygen bond distances of 3.0-3.6 Å were chosen to match the established range seen in ion-association to Lindqvist ions (Table S7-S9).⁶ However, unlike the bonding of Cs⁺ to the faces of the {Nb₆} superoctahedron,⁷ Cs⁺ instead associates more loosely to bridging and terminal oxygen atoms in the currently studied niobo-tungstate clusters. The cation-only coordination environments with clusters removed are also highlighted (Figure S10).

3.3 Stability and Isomer Confirmation by ESI-MS

Electrospray-ionization mass-spectrometry (ESI-MS) was employed to explore the stability and confirm isomeric purity of the

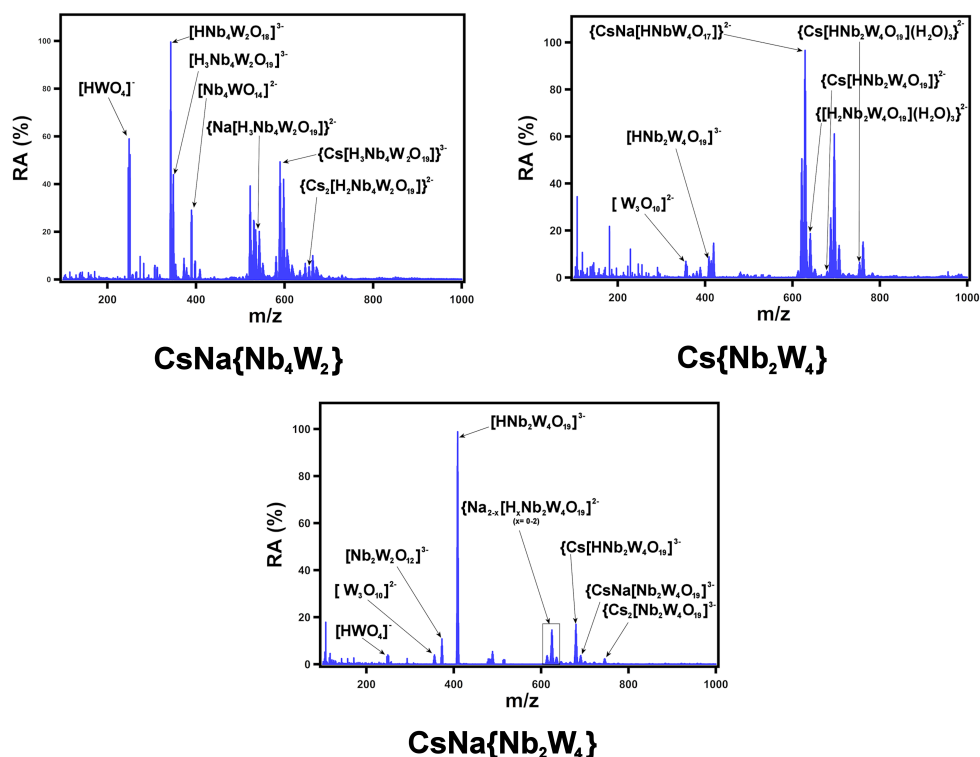


Fig. 5 ESI-MS spectra of CsNa{Nb₄W₂}, Cs{Nb₂W₄}, and CsNa{Nb₂W₄}.

three compounds in solution and in the gas phase. This is also the most effective method to distinguish between a pure phase of mixed-metal clusters, and a mixture of co-crystallized clusters of different compositions. Spectra of CsNa{Nb₄W₂}, Cs{Nb₂W₄}, and CsNa{Nb₂W₄} were obtained in aqueous solution. The regions of interest in these spectra, along with labeled peak envelopes are shown in Figure 5, while Table S14 summarizes the assignments for these peak envelopes.

The spectrum of CsNa{Nb₄W₂} confirms the formula of the cluster as determined by crystallography and elemental analysis. Four peak envelopes can be assigned to the cluster, protonated and associated to Cs⁺ and Na⁺ counteractions to different degrees. The envelope displaying the highest intensity is ascribed to an incomplete monoprotinated cluster in which one of the oxo ligands is missing. Hexacoltanate species in the gas phase missing one or more oxo ligands are fairly common, as reported in previous mass spectrometry studies.³² The high relative intensity of the [HWO₄]⁻ peak, when compared to the spectra discussed below, suggests that this polyanion is less stable in the gas phase than {Nb₂W₄}.

The spectra of the two salts of {Nb₂W₄} also confirm the crystallographic/EDX formula despite the differences in the relative intensity of a number of peak envelopes. Seven and four peaks in the CsNa{Nb₂W₄} and Cs{Nb₂W₄} spectra respectively can be

Table 3 λ_{max} values for $n(O_b) \rightarrow \pi^*(M-O_b)$ transitions in members of the [Nb_xW_{6-x}O₁₉]^{(2+x)-} series

Anion	λ_{max} , nm
{Nb ₆ }	248
{Nb ₄ W ₂ }	253
{Nb ₂ W ₄ }	269, 271 ^a
{W ₆ }	278 ³³

^a CsNa{Nb₂W₄} and Cs{Nb₂W₄}, respectively.

assigned to an intact {Nb₂W₄} polyanion. The peaks showing the highest intensity in each spectrum are ascribed to a protonated intact cluster in the case of the CsNa{Nb₂W₄} spectrum and to an adduct, formed by Cs⁺ and adventitious Na⁺ counteractions associated to a protonated {Nb₂W₄} cluster missing two oxo ligands, in the case of the Cs{Nb₂W₄} spectrum. Interestingly, the presence of a [W₃O₁₀]²⁻ fragment in both {Nb₂W₄} spectra confirms the spectroscopic assignment of this cluster as the cis-isomer.

3.4 Electronic Structure Trends by UV-Vis Spectroscopy

As tungsten occupancy in the isostructural [Nb_xW_{6-x}O₁₉]^{(2+x)-} series increases, a monotonic redshift trend is observed in the $n(O_b) \rightarrow \pi^*(M-O_b)$ transfer band (Table 3, Figure 6). This can be attributed to the $\pi^*(Nb-O_b)$ LUMO³⁴ in {Nb₆} being higher-

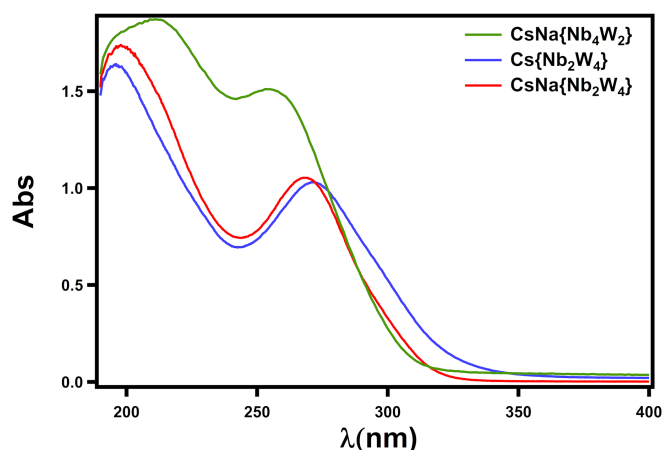


Fig. 6 UV-visible spectra of CsNa{Nb₄W₂}, Cs{Nb₂W₄}, and CsNa{Nb₂W₄} (0.1 mM aqueous solutions). The higher-wavelength peaks correspond to $n(\text{O}_b) \rightarrow \pi^*(\text{M}-\text{O}_b)$ charge transfer bands.

Table 4 λ_{max} values for $n(\text{O}_b) \rightarrow \pi^*(\text{M}-\text{O}_b)$ transitions in $[\text{M}_6\text{O}_{19}]^{n-}$ (M = Nb, Mo, Ta, W)

	Group V, λ_{max}	Group VI, λ_{max}
4d	[Nb ₆ O ₁₉] ⁸⁻ , 248 nm	[Mo ₆ O ₁₉] ²⁻ , 326 nm
5d	[Ta ₆ O ₁₉] ⁸⁻ , 215 nm	[W ₆ O ₁₉] ²⁻ , 278 nm

lying (more destabilized) than the $\pi^*(\text{W}-\text{O}_b)$ LUMO in {W₆} with respect to their $n(\text{O}_b)$ HOMOs.³⁵ The higher-lying LUMO arises from the poorer mixing of Nb_{4d} than W_{5d} atomic orbitals with O_b, due to their atomic orbital energies being further apart.³⁶ The λ_{max} values in the $n(\text{O}_b) \rightarrow \pi^*(\text{M}-\text{O}_b)$ transitions for two other prominent hexametalate species, [Ta₆O₁₉]⁸⁻ and [Mo₆O₁₉]²⁻, are 215 nm and 326 nm, respectively.^{34,37} Comparing these transitions to those in {Nb₆} and {W₆}, the redshift across a period is larger than the blueshift going down a group (Table 4). This arises from the significant lowering of atomic orbital energies due to the additional proton in each Group VI metal center (e.g., from Ta to W). The relative similarity in energy allows W_{5d} orbitals to have better π -mixing with oxygen's 2p orbitals. This stabilizing effect is greater than the destabilization resulting from poorer orbital overlap of the 5d orbitals with 2p orbitals, compared to 4d orbitals in the same group (e.g., from Nb to Ta) with 2p orbitals. The absorption peak positions of the niobo-tungstate clusters are indicative of the mixed occupancy of niobium and tungsten at each metal site, constituting an intermediate level of M_{nd}-O_b orbital mixing. This results in the LUMOs for the mixed-metal species lying between those in {Nb₆} and {W₆}, with greater tungsten occupancy resulting in smaller energy gaps. The electronic properties of these mixed Nb/W POMs are thus indicative of hybrids of {Nb₆} and {W₆}.

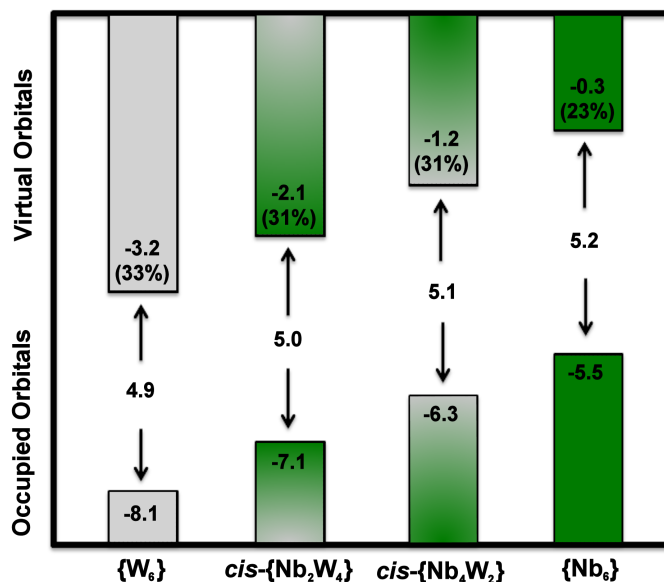


Fig. 7 HOMO, LUMO, and E_{gap} energies of CsNa{Nb₄W₂}, Cs{Nb₂W₄}, and CsNa{Nb₂W₄} in eV. The O_b atomic orbital contributions to the LUMOs are shown in parentheses.

3.5 Computational Characterization

The electronic structure and properties of both cis- and trans-isomers of {Nb₄W₂} and {Nb₂W₄} were studied using first-principles calculations at the PBE and B3LYP levels of theory (Tables S21-S22). Identifying the proper isomers of each structure is complicated by the crystallographic disorder of these highly-symmetric species, warranting verification by computational methods. The relative electronic energies for the cis- and trans-isomers of {Nb₄W₂} and {Nb₂W₄} indicated slightly greater stability (on the order of 1-2 kcal·mol⁻¹) in the cis-isomer of each structure, confirming the predictions from IR spectra and group theory (Table S20).

The historically well-characterized {Nb₆} and {W₆} structures were also investigated in order to properly elucidate the mixed-metal polyanions in the context of their intermediate properties between those of their single-metal congeners. In each hexametalate structure, the HOMO and LUMO are composed of the occupied O_{2p} and empty antibonding $\pi^*(\text{M}-\text{O}_b)$ orbitals, respectively. Combining Nb and W within the same structure resulted in intermediate electronic structures between the two pure hexametalate species, as predicted by the UV-vis spectra. Increased Nb occupancy resulted in greater energy gaps due to generally poorer mixing between M_{nd} and O_{2p} atomic orbitals (Figure 7, Table S23). This poor mixing arises from the disparate atomic orbital energies of Nb_{4d} and O_{2p} (-2.95 eV and -9.82 eV for a niobium atom and an oxygen atom, respectively) and results in higher-lying LUMOs with less O_{2p} character. The energy required

Table 5 Experimental and calculated (B3LYP) energy gaps (E_{gap}) for $\{\text{Nb}_6\}$, $\{\text{Nb}_4\text{W}_2\}$, $\{\text{Nb}_2\text{W}_4\}$, and $\{\text{W}_6\}$

Cluster	Calc. E_{gap} (eV)	Calc. Excitation Energy (eV) ^a	Exp. E_{gap} (eV) ^b
$\{\text{Nb}_6\}$	5.278	4.451	4.999
$\{\text{Nb}_4\text{W}_2\}$	5.082	4.419	4.901
$\{\text{Nb}_2\text{W}_4\}$	5.011	4.347	4.609, 4.575 ^c
$\{\text{W}_6\}$	4.876	4.235	4.460

^a Average excitation energy (3 lowest excitations) from TD-DFT calculations.

^b Calculated as $E = \frac{hc}{\lambda}$, where λ is the value of wavelength for the absorption ascribed to the $n(\text{O}_b) \rightarrow \pi^*(\text{M-O}_b)$ charge transfer across bridging oxygen bonds.

^c CsNa $\{\text{Nb}_2\text{W}_4\}$ and Cs $\{\text{Nb}_2\text{W}_4\}$, respectively.

to promote electrons from the fully- O_{2p} nonbonding orbitals is thus increased. The atomic orbital energy of W_{5d} is closer to that of O_{2p} (-4.34 eV for a tungsten atom), resulting in LUMOs with more O_{2p} character.

Our calculated HOMO-LUMO gaps are overestimated by both PBE and B3LYP with respect to those inferred by the UV-Vis spectra (Table 5). This disparity can be attributed to the dependency of the molecular orbital energies, and hence the HOMO-LUMO gap, on the DFT functional.³⁸ Nonetheless, the trend of smaller HOMO-LUMO gaps with increasing tungsten occupancy is maintained in all forms of computational and experimental characterization.

4 Conclusions

Through a combination of experimental and computational methods, three cesium salts of members of the $[\text{Nb}_x\text{W}_{6-x}\text{O}_{19}]^{(2+x)-}$ series were shown to exhibit intermediate solid-state bond distances and electronic properties between those of Group V and Group VI POMs. Their resultant properties highlight the nature of their mixed character. By combining these two disparate classes of POMs, advanced materials with unique, hybrid properties are attainable from water. The potential thus arises for tuning the solubility and base-catalytic capabilities of Group V POMs with the electrochemical activity of Group VI POMs, among other properties. In order to fully harness this, the requisite understanding of structures from this study must be supplemented by aqueous state evaluation of self-assembly and ion-pairing patterns, especially with Cs^+ . ^{133}Cs T_1 inversion-recovery experiments are underway to evaluate the relative degrees of contact ion-pairing between various Group V and VI mixed-metal POMs and Cs^+ . This association data can then be related to electronic structures and solubilities. Additionally, solution-state thermochemical measurements are in progress to evaluate the energetic differences between the solid and aqueous states of POMs. The results of our ongoing investigations on these topics will be presented in future publications.

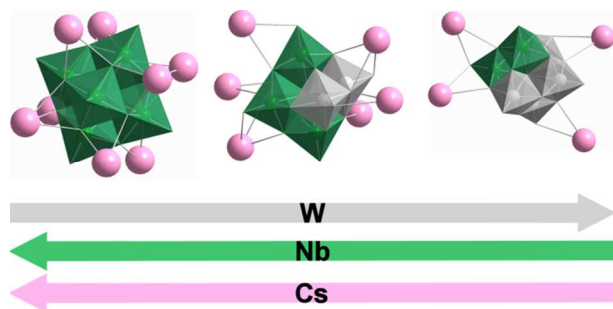
5 Acknowledgements

This work was supported by the U.S. Department of Energy, Office of Basic Energy Sciences, Divisions of Materials Sciences and Engineering, under award DE-SC0010802. P. Miró thanks Thomas Heine for the scientific discussions and support on the computational characterization.

References

- L. C. Baker and D. C. Glick, *Chemical reviews*, 1998, **98**, 3–50.
- H. N. Miras, J. Yan, D.-L. Long and L. Cronin, *Chemical Society Reviews*, 2012, **41**, 7403–7430.
- M. Nyman, *Dalton Transactions*, 2011, **40**, 8049–8058.
- Y. Marcus and G. Hefter, *Chemical reviews*, 2006, **106**, 4585–4621.
- T. M. Anderson, S. G. Thoma, F. Bonhomme, M. A. Rodriguez, H. Park, J. B. Parise, T. M. Alam, J. P. Larentzos and M. Nyman, *Crystal growth & design*, 2007, **7**, 719–723.
- M. R. Antonio, M. Nyman and T. M. Anderson, *Angewandte Chemie*, 2009, **121**, 6252–6256.
- M. Nyman, T. M. Alam, F. Bonhomme, M. A. Rodriguez, C. S. Frazer and M. E. Welk, *Journal of Cluster Science*, 2006, **17**, 197–219.
- M. R. Antonio, M. Nyman and T. M. Anderson, *Angewandte Chemie*, 2009, **121**, 6252–6256.
- P. Molina, D. Sures, P. Miró, L. Zakharov and M. Nyman, *Dalton Transactions*, 2015, **44**, 15813–15822.
- M. Pope and B. Dale, *Q. Rev. Chem. Soc.*, 1968, **22**, 527–548.
- B. Spinner, *Rev. Chim. Miner.*, 1968, **5**, 839–868.
- D. Tsumune, T. Tsubono, M. Aoyama and K. Hirose, *Journal of environmental radioactivity*, 2012, **111**, 100–108.
- O. Oms, A. Dolbecq and P. Mialane, *Chemical Society Reviews*, 2012, **41**, 7497–7536.
- A. Proust, B. Matt, R. Villanneau, G. Guillemot, P. Gouzerh and G. Izzet, *Chemical Society Reviews*, 2012, **41**, 7605–7622.
- U. Kortz, A. Mueller, J. van Slageren, J. Schnack, N. S. Dalal and M. Dressel, *Coordination Chemistry Reviews*, 2009, **253**, 2315–2327.
- M. S. Balula, J. A. Gamelas, H. M. Carapuça, A. Cavaleiro and W. Schlindwein, *European Journal of Inorganic Chemistry*, 2004, **2004**, 619–628.
- v. J. Fuchs, W. Freiwald and H. Hartl, *Acta Crystallographica Section B: Structural Crystallography and Crystal Chemistry*, 1978, **34**, 1764–1770.
- M. Dabbabi and M. Boyer, *Journal of Inorganic and Nuclear Chemistry*, 1976, **38**, 1011–1014.
- K. Bouadjadja-Rohan, C. Lancelot, M. Fournier, A. Bonduelle-Skrzypczak, A. Hugon, O. Mentré and C. Lamonnier, *European Journal of Inorganic Chemistry*, 2015, **2015**, 2067–2075.
- F. Bannani, H. Driss, R. Thouvenot and M. Debbabi, *Journal of Chemical Crystallography*, 2007, **37**, 37–48.
- M. C. K. França, J.-G. Eon, M. Fournier, E. Payen and O. Mentré, *Solid State Sciences*, 2005, **7**, 1533–1541.
- V. Day, W. Klemperer and C. Schwartz, *Journal of the American Chemical Society*, 1987, **109**, 6030–6044.
- Y. Hou, L. N. Zakharov and M. Nyman, *Journal of the American Chemical Society*, 2013, **135**, 16651–16657.
- T. Kojima, M. R. Antonio and T. Ozeki, *Journal of the American Chemical Society*,

- 2011, **133**, 7248–7251.
- 25 L. B. Fullmer, R. H. Mansergh, L. N. Zakharov, D. A. Keszler and M. Nyman, *Crystal Growth & Design*, 2015, **15**, 3885–3892.
- 26 C. W. Balke and E. F. Smith, *Journal of the American Chemical Society*, 1908, **30**, 1637–1668.
- 27 C. Rocchiccioli-Deltcheff, R. Thouvenot and M. Dabbabi, *Spectrochimica Acta Part A: Molecular Spectroscopy*, 1977, **33**, 143–153.
- 28 G. J. Palenik, *Inorganic chemistry*, 1997, **36**, 3394–3397.
- 29 R. M. Wood and G. J. Palenik, *Inorganic chemistry*, 1998, **37**, 4149–4151.
- 30 S. M. Kanowitz and G. J. Palenik, *Inorganic Chemistry*, 1998, **37**, 2086–2088.
- 31 K. Tytko, J. Mehmke and S. Fischer, 1999, 129–321.
- 32 F. Sahureka, R. C. Burns and E. I. von Nagy-Felsobuki, *Inorganica chimica acta*, 2003, **351**, 69–78.
- 33 Y. Ding, W. Zhu, H. Li, W. Jiang, M. Zhang, Y. Duan and Y. Chang, *Green Chemistry*, 2011, **13**, 1210–1216.
- 34 G. J.-P. Deblonde, A. Moncomble, G. Cote, S. Bélair and A. Chagnes, *RSC Advances*, 2015, **5**, 7619–7627.
- 35 J. Li, *Journal of cluster science*, 2002, **13**, 137–163.
- 36 L. Yan, X. López, J. J. Carbó, R. Sniatynsky, D. C. Duncan and J. M. Poblet, *Journal of the American Chemical Society*, 2008, **130**, 8223–8233.
- 37 M. Araghi, V. Mirkhani, M. Moghadam, S. Tangestaninejad and I. Mohammdpoor-Baltork, *Dalton Transactions*, 2012, **41**, 3087–3094.
- 38 D. Ravelli, D. Dondi, M. Fagnoni, A. Albini and A. Bagno, *Physical Chemistry Chemical Physics*, 2013, **15**, 2890–2896.



The physical and electronic structures of cesium salts of niobo-tungstate Lindqvist ions vary with Nb content, elucidated experimentally and computationally.